J. Fluid Mech. (1984), *vol.* 145, *pp.* 253–273
Printed in Great Britain

Wind-induced entrainment in a stably stratified fluid

By C. KRANENBURG

Laboratory of Fluid Mechanics, Department of Civil Engineering,
Delft University of Technology, 2628CN Delft, The Netherlands

(Received 2 June 1983 and in revised form 2 April 1984)

Experiments on mixed-layer deepening in a straight wind flume initially containing a two-layer fluid were carried out. In order to simulate an effectively unlimited water body, or a situation where the presence of endwalls is not yet noticeable, the water from the upper layer was withdrawn at the downstream end, and supplied again at the upstream end in part of the experiments. Upper-layer depths, and mean-density and mean-velocity profiles were measured for overall Richardson numbers (based on the surface friction velocity) ranging from 22 to 1090. Gradient Richardson numbers in the transition layer (between the mixed layer and the undisturbed layer) and in the mixed layer were estimated. The correction of the results for the effects of recirculation is discussed.

1. Introduction

Wind action at the free surface of a stably stratified water basin forms a turbulent upper layer, which deepens in the course of time as denser water from the undisturbed layer is entrained into the upper layer. Within the upper layer, a layer usually assumed to be well-mixed and a transition layer between mixed and undisturbed layers can be distinguished. Buoyancy and horizontal velocity vary markedly across the transition layer so that turbulence is greatly suppressed by buoyancy differences. Heating, cooling and Coriolis force can interact with the mechanical wind-mixing process.

The entrainment mechanism is different for a situation where the presence of endwalls of the basin is not yet noticeable, and the situation where wind set-up has created a streamwise pressure gradient. In the former case the transition layer is relatively deep and the entrainment rate is relatively large. When the reflection of internal waves from the endwalls has led to a quasi-steady state with the wind shear stress balanced by a pressure gradient, the mean upper-layer velocity vanishes and the transition layer becomes relatively shallow. In this phase of the mixing process the entrainment rate is much less than in the previous phase. These and other aspects of mixed-layer dynamics are discussed, among others, by Spigel & Imberger (1980) and Imberger & Hamblin (1982). These authors also review the earlier literature.

Beside field measurements, laboratory experiments have been a major source of insight into turbulent-entrainment processes. To avoid unwanted endwall effects, Kato & Phillips (1969), Kantha, Phillips & Azad (1977) and Deardorff & Willis (1982) carried out experiments in annular tanks to simulate one-dimensional entrainment processes of large horizontal extent. The experiments of Scranton & Lindberg (1983) seem to indicate, however, that results obtained in annular tanks should be used with care, since channel curvature causes secondary flow and pronounced radial

stratification of density, momentum and turbulent kinetic energy. A procedure to extrapolate the results to a situation with zero curvature seems to be unknown.

A second, but less serious, problem arising in interpreting entrainment experiments without endwall effects is the way sidewall friction influences the results. Price (1972*a*) and Thompson (1979) extrapolated the entrainment rates observed by Kato & Phillips and Kantha *et al.* to the case of zero aspect (depth of upper layer to width of channel) ratio. Kranenburg (1983) employed a simple analytical model of the entrainment process, including sidewall friction, and analysed the experiments of Kato & Phillips, Kantha *et al.*, Deardorff & Willis and Moore & Long (1971). These studies indicate that, in the experiments mentioned, sidewall friction substantially reduces entrainment rates and mean velocities, in particular in very stable flows. The experiments of Jones & Mulhearn (1983) were also affected by this difficulty. As a secondary effect the duration of an experiment can become so long that viscous shear stresses set up an accelerating flow in the 'undisturbed' lower layer. The reduced velocity difference across the transition layer may further decrease the entrainment rate. The extrapolated results for zero aspect ratio agree, at least in a qualitative sense, with certain second-order turbulence models (Mellor & Strub 1980; Kundu 1980, 1981) and integral entrainment models (see e.g. Spigel & Imberger 1980). Since entrainment models use to be calibrated partly on the basis of the annular-tank experiments mentioned, however, there is a need for an experiment in which streamline curvature is absent.

The present study is concerned with the mechanical aspects of wind mixing in the phase where the endwalls do not yet affect the entrainment process.† The apparatus used is a straight wind flume in which a two-layer system was set up before an experiment was started. The presence of endwalls limits the duration of an experiment, and it is necessary to extend it at larger values of Ri_*, where

$$Ri_* = \frac{\Delta\rho_0}{\rho_r}\frac{gH_0}{u_*^2}.$$

Here ρ_r is a reference density of water, $\Delta\rho_0$ the initial density difference between the layers, g the gravitational acceleration, H_0 the initial depth of the upper layer and u_* the surface-friction velocity related to the wind shear stress. To extend the time available, the water transported in the upper layer was selectively withdrawn at the downstream end, pumped back through a pipe beside the flume, and discharged smoothly at the upstream end. Some additional mixing caused by this procedure has to be taken into account. The homogeneous lower layer was to stay at rest during an experiment in which the upper layer was recirculated. The rate of recirculating flow could be increased approximately linearly in time, as in a situation where sidewall friction is absent. The duration of the experiments was relatively short, and viscous effects in the lower layer were almost absent. A more detailed description of the wind flume, instrumentation used and experimental procedure is given in §2. Results of preliminary experiments dealing with the measurement of the surface shear stresses are also presented in §2. In the entrainment experiments upper-layer depths, and mean-density and mean-velocity profiles were measured (§§3.1 and 3.2). The entrainment rates and gradient Richardson numbers observed in the experiments with recirculation are corrected for the influence of entrance mixing in §3.3.

† Experiments with the wind shear stress balanced by a streamwise pressure gradient (as made by Wu 1973) will be reported elsewhere.

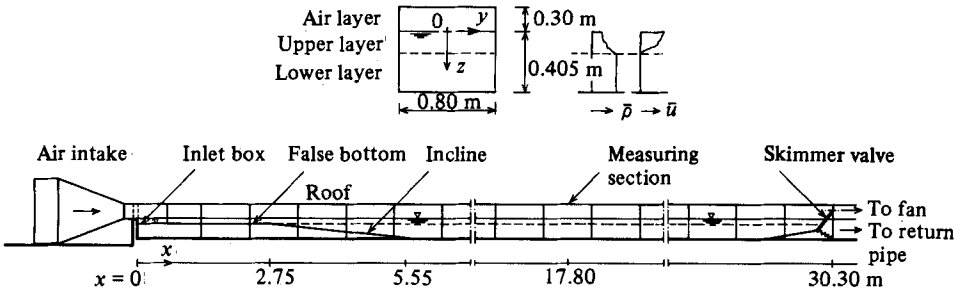

FIGURE 1. Diagrams of wind flume (experiments with recirculation), cross-section, density and velocity profiles, and coordinate system. Note different scales.

2. Experimental set-up and determination of surface shear stress

2.1. *Wind flume*

The experiments were carried out in a wind flume, effective length 32.50 m (experiments without recirculation) or about 27 m (experiments with recirculation), width 0.80 m, depth of air layer 0.30 m, and water depth 0.405 m. The flume had a plywood roof over its total length, glass sidewalls and a plastered bottom (figure 1). A fan sucked air through an air intake constructed at the upstream endwall. The air velocities $u_{0.1}$ at 0.1 m above the water surface varied from about 4 to 11 m/s. Roughness elements were placed in the air intake to increase the turbulence intensity of the inflowing air. In preliminary experiments wind waves were found to develop when the air velocity was larger than about 6 m/s. The wave heights were extremely large when compared with the depth of the upper layer (initially 0.10 m) and excessive mixing resulted. To eliminate this unwanted scale effect the wind waves were suppressed for the greater part by adding 500 cm^3 of a surfactant (a detergent, Teepol, Shell) to the upper layer. Mitsuyasu & Honda (1982) examined the effects of a surfactant in greater detail. It will be explained in §2.4 that adding the surfactant did not noticeably alter the surface shear stress.

Apart from wind waves, some seiching (sloshing) of the water body in the flume was observed when the wind started to blow, but the seiching did not interact with the internal mixing process.

Sodium chloride dissolved in tap water was used to obtain the density differences between upper and lower layers. The relative density differences varied from 0.005 to 0.039. The two-layer stratification was set up by first letting the fresh upper-layer water into the flume, and then, after a stilling period, the denser lower-layer water was slowly supplied through diffusers mounted in the bottom. The filling process took several hours, and after filling, the interface had thickened to some centimetres owing to molecular diffusion.

The system for recirculating the water transported in the upper layer consisted of a 'skimmer valve' at the downstream end of the flume used to selectively withdraw the upper-layer water (figure 1), a pump, a return pipe beside the flume, inner diameter 75 mm, in which a butterfly valve was mounted near the skimmer valve, and an inlet box (figure 1) at the upstream end.

The skimmer valve consisted of an aluminium plate, of width almost equal to that of the flume and of height about 0.15 m, placed below the free surface so as to stem the lower layer and to make possible the withdrawal from the upper layer. On either side the plate had arms and hinges attached to the sidewalls of the flume to allow

for adaptation of the height of the valve to the level of the interface, which gradually dropped during an experiment. To prevent leakage from the lower layer the plate was connected to sidewalls and bottom by means of bellows. A small incline was attached to the lower edge of the plate to suppress undesired vortex generation when the valve was adjusted.

The inlet box, of inner height 85 mm, was mounted flush with the free surface, spanned the width of the flume, was supplied with perforated plates to spread the inflow from the return pipe, and was connected to a horizontal false bottom, of length 2.15 m. This bottom passed into an incline, of slope 1:10, to reduce entrance mixing with water from the lower layer as much as possible. This set-up nevertheless caused some additional mixing that has to be considered when analysing the results. The recirculation system was filled with fresh water before an experiment was started. The maximal rate of recirculating flow was about 0.026 m^3/s. The way in which the (time-dependent) rate of recirculating flow was prescribed will be discussed in §2.3.

2.2. *Instrumentation*

In preliminary experiments laser-Doppler velocimetry was used to measure mean-velocity profiles in air and (homogeneous) water layers. Horizontal pressure differences in these layers were measured between two cross-sections, 15 or 22 m apart, using a pressure-difference transducer. These measurements served to determine the surface shear stresses.

In order to minimize the influence of the endwalls and recirculation, the measurements during the entrainment experiments were done in a measuring section near the middle of the flume ($x = 17.80$ m, coordinates are indicated in figure 1). Upper-layer depths were obtained by filming the shadowgraph image of the density structure projected on the sidewall of the flume. Mean-velocity profiles were obtained by periodically releasing small oil drops slightly less dense than fresh water from the bottom of the flume. The shadows of the rising drops were also filmed.

The velocity profiles were determined from the horizontal displacements of a large number of oil drops. An alternative would have been to use hot-film velocimetry, but serious contamination problems were expected in the open system used. In one experiment oil drops were released at 0.05, 0.10 and 0.15 m from the sidewall and also in the centreline of the flume to examine the spanwise velocity distribution. The distance from the wall could not be too large for the drops to remain visible on the film. On the other hand, wall influence on the vertical velocity profiles was to be avoided. A distance of 0.15 m from the sidewall was found to meet both requirements.

Conductivity profiles were taken in the centreline of the flume at $x = 17.80$ m. Conductivities were converted into densities by calibrating. The conductivity probe used was designed to take mean-density profiles. To this end, electrodes, of length 120 mm and thickness 2 mm, were placed in a horizontal position and normal to the flow. Contamination problems were avoided by using carbon electrodes. The response time of the probe could be reduced by employing two pairs of electrodes. One pair served to induce an electric field excited at 2 kHz, and the second pair to measure the resistance of the fluid. The amplitude-modulated signal from the latter pair was rectified, inverted using a divider to give conductivity, and amplified. The probe could be traversed vertically through the upper 0.30 m of the water layer at a velocity of ± 20 mm/s. The near-linear output was sampled, stored in the memory of a microcomputer, and recorded on a strip-chart recorder.

The microcomputer was also used to produce signals to start (and stop) at preselected times the dosing of oil drops, filming, and the traversing of the conductivity probe.

The flow rate in the return pipe was measured using an orifice plate and a pressure-difference transducer. It was monitored on a voltage meter and recorded on the strip-chart recorder.

The accuracy of the surface friction velocities (§2.4) is about $\pm 5\,\%$. The depth of the upper layer was read with an accuracy of about $\pm 5\,\%$, and that of the transition layer with an accuracy of about $\pm 10\,\%$. The accuracy of the density profiles was improved by averaging the values measured during upward and downward motion of the probe. Thus the effect of the dragging along of ambient fluid was reduced. The accuracy of the averaged densities is thought to be about $\pm 4\,\%$ of the initial density difference between the layers. The accuracy of the horizontal velocities deduced from the motions of the rising oil drops is about ± 10 mm/s. The accuracy of the gradient Richardson numbers in the transition layer is about $\pm 15\,\%$. The temperature differences between upper and lower layers did not exceed 1 °C.

2.3. *Method used to control the rate of recirculating flow*

If sidewall friction were absent, the equation of motion for the upper layer would be

$$\frac{\mathrm{d}}{\mathrm{d}t}(UH) = u_*^2, \tag{2.1}$$

where t is time, U the mean upper-layer velocity and H the upper-layer depth. The instant at which the shear stress becomes effective is chosen as $t = 0$. This event lags behind the start of the wind, since it takes some time before turbulence starts to develop in the upper layer. On integration, (2.1) then gives for the flow rate $Q(t)$ in the upper layer, with $Q(0) = 0$,

$$Q(t) = UHW = Wu_*^2\, t, \tag{2.2}$$

where W is the width of the flume.

The butterfly valve in the return pipe was controlled by hand such that the rate Q_r of recirculating flow was equal to $Q(t)$ given by (2.2), but, if there was a threat of withdrawal of water from the lower layer at the skimmer valve, Q_r was reduced, by preference temporarily, below $Q(t)$. The flow near the skimmer valve was observed using the shadowgraph technique and a sensitive vane placed in the lower layer. The actual rate of recirculating flow was read on the voltage meter mentioned and compared with the flow rate $Q(t)$ desired. Obviously this procedure requires some skill, but after experience had been gained with a particular experiment the method appeared quite successful and Q_r closely approximated $Q(t)$ (however, see also §3.2). Each experiment was repeated one or two times to test the reproducibility. The results of the final experiments are discussed in §3.2.

Sidewall friction would tend to reduce the flow rate $Q(t)$. Since it was nevertheless possible in most experiments to withdraw a flow rate close to that given by (2.2), a streamwise pressure gradient may have gradually developed during an experiment, so that the upper-layer depth would become a function of x. However, entrance mixing caused by recirculation may also play a part here, since it tends to increase the flow rate in the upper layer.

2.4. *Determination of surface shear stress*

In a series of preliminary experiments with an unstratified water layer, no recirculation, steady-state conditions and fully developed turbulence, velocity profiles in air and water layers were taken and mean surface shear stresses were determined from pressure-difference measurements. The results obtained are comparable to those of Wu (1975) and Phillips & Banner (1974).

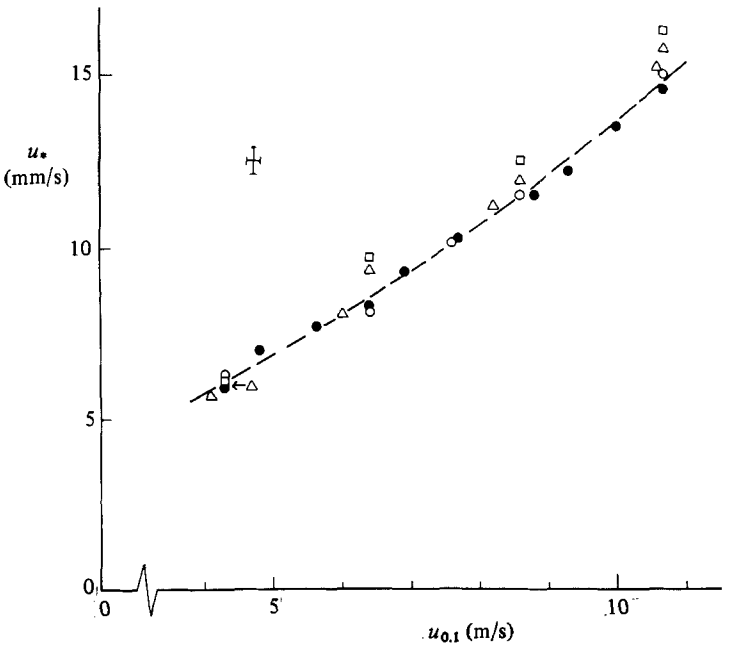

FIGURE 2. Surface friction velocity : △, from velocity profiles in air layer ($x = 17.80$ m); □, from velocity profiles in water layer ($x = 17.80$ m); ○, from pressure differences measured over 15 m; ●, from pressure differences measured over 22 m; ---, smooth curve (mean friction velocities).

The uniformity of the flow in the air layer was tested by taking three mean-velocity profiles near the middle of the flume ($x = 17.80$ m; $y = -0.20, 0, +0.20$ m) and closer to the upstream end ($x = 9.80$ m; $y = -0.20, 0, +0.20$ m). The profiles at $x = 9.80$ m appeared to be somewhat less uniform than those at $x = 17.80$ m; in both cross-sections the profiles were approximately logarithmic. Friction velocities u_{*a} ($= (\tau_s/\rho_a)^{\frac{1}{2}}$, where τ_s is the surface shear stress and ρ_a the air density) were determined from the gradients of the profiles at $x = 17.80$ m assuming von Kármán's constant to be equal to 0.41. Since wave drag is negligible here (see below) equivalent friction velocities u_* ($\rho_r u_*^2 = \rho_a u_{*a}^2$) for the water layer can be calculated. These u_* values are shown in figure 2 (triangles).

Mean-velocity profiles in the homogeneous water layer were taken near the middle of the flume ($x = 17.80$ m; $y = -0.20, 0, +0.20$ m). The profiles in the upper 0.20 m were approximately logarithmic. Friction velocities u_* were determined as indicated above. These u_* values, which are also shown in figure 2 (squares), are close to those obtained for the air layer, but tend to be even somewhat larger. It is therefore concluded that wave drag, which would decrease the friction velocity in the water layer below that in the air layer, is negligible. This is not surprising, since wind waves were suppressed for the greater part.

The friction velocities obtained from the observed velocity profiles are local values. Friction velocities averaged over a large part of the free surface, which are more suitable input parameters of the entrainment experiments, were obtained by measuring streamwise pressure differences in the water layer. It can be shown that sidewall and bottom friction are negligible here when compared with the surface shear stress. A balance of forces then gives

$$u_*^2 = a \frac{1}{\rho_r} \frac{\partial \bar{p}}{\partial x}, \tag{2.3}$$

where a is the water depth and $\partial\bar{p}/\partial x$ the mean streamwise pressure gradient calculated from the pressure-difference measurements. The calculated friction velocities are shown in figure 2 (circles).

In one experiment wind waves were allowed to develop and the mean pressure difference was recorded continuously when the air velocity was $u_{0.1} = 7.6$ m/s. After a steady-state situation had become established, 200 cm^3 of surfactant was released at the free surface near the air intake. The surfactant damped the wind waves almost completely as it spread over the free surface. Any influence on the mean pressure difference was not observed, however. This and other results obtained indicate that a small amount of surfactant did not noticeably alter the transfer of shear stresses across the free surface.

A possible effect of stratification of the water layer on the surface shear stress was examined in various ways. First, the pressure gradient in the upper layer of a two-layer fluid was measured when wave reflections from the endwalls had become damped so that a quasi-steady set-up situation had developed (no recirculation was applied). The friction velocity follows from an expression like (2.3). However, the water depth a has to be replaced by the depth of the upper layer, or, more precisely, the depth where the shear stress vanishes. This depth was difficult to estimate, so that the friction velocities thus determined are not accurate. It was found that $u_* \approx 8.3$–9.1 mm/s when $u_{0.1} = 6.4$ m/s, and $u_* \approx 11.6$–12.8 mm/s when $u_{0.1} = 8.6$ m/s. These friction velocities seem to be slightly larger than those of figure 2 (circles), but presumably the differences are not significant. Furthermore, the pressure difference had to be measured close to the downstream end of the flume because of set-up of the upper layer. The friction velocities obtained in this way may therefore not be representative of the whole free surface. Another experiment also indicating that, within the accuracy reached, stratification does not noticeably affect the friction velocity is described in §3.

Since it decreases the velocity difference between the air layer and the free surface, recirculation should in principle cause some reduction in the friction velocities. To account for this effect a quadratic resistance law is assumed, so that the friction velocities under homogeneous conditions are reduced by a factor

$$\frac{u_{0.1} - U}{u_{0.1}},$$

where $U = Q_r/WH$. This factor is close to 1 (between 0.96 and 1) for the experiments described in §3.2.

3. Entrainment experiments

3.1. *Experiments without recirculation*

In the experiments without recirculation (table 1) the endwalls generate external and internal waves. The external waves cause the net flow rate (that is, the sum of the flow rates in upper and lower layers) to be zero, apart from oscillatory motions caused by seiching. As a result a (laminar) flow against the wind develops in the lower layer. Internal surges effectively nullifying the mean horizontal velocities in both layers start to propagate from either endwall after the wind has started to blow. As a consequence, there is only a certain period available (three to five minutes, depending on the experimental conditions) during which the internal mixing process near the middle of the flume is not influenced by the endwalls.† The limited duration of this

† Thorpe (1968) described a similar process, though on a much smaller scale, in a study of Kelvin–Helmholtz instability of a two-layer fluid in an inclined duct.

Experiment	$u_{0.1}$ (m/s)	u_* (mm/s)	H_0 (m)	$\frac{\Delta\rho_0}{\rho_r}$	Ri_*
1	10.7	14.8	0.10	0.0048	22
2	8.6	11.4	0.10	0.0053	40
3	7.6	10.1	0.10	0.0050	47
4	6.4	8.4	0.10	0.0048	67
5	8.6	11.4	0.20	0.0050	75
6	6.4	8.4	0.10	0.010	140

TABLE 1. Experiments without recirculation

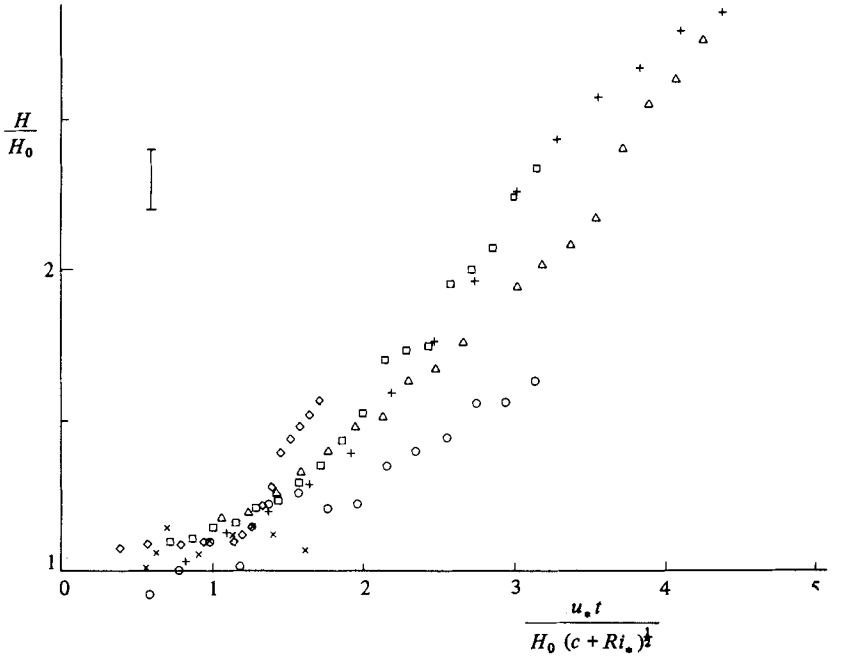

FIGURE 3. Upper-layer depths in experiments without recirculation: +, experiment 1; △, 2; □, 3; ○, 4; ◇, 5; ×, 6.

period sets an upper bound to the overall Richardson number Ri_*, since the time interval necessary for the entrainment mechanism to become fully developed increases with Ri_* (see below). In experiment 6, for example, Ri_* was about 140 and no mixing was observed near the middle of the flume during the time available (about 230 s, figure 3).

Because of the restrictions imposed on Ri_* and the duration of an experiment, sidewall friction is negligible in these experiments.

The relative depths H/H_0 of the upper layer as determined from the filmed shadowgraph images are shown in figure 3. Time has been non-dimensionalized so as to produce a collapse of data according to the integral entrainment model of Spigel & Imberger (1980). Figure 3 suggests that initially the entrainment rates are very small (in certain instances the initial variations in upper-layer depth are caused by internal waves). The duration of this period is given by, to an order of magnitude,

$$t_1 = \frac{H_0}{u_*}(c + Ri_*)^{\frac{1}{2}}, \tag{3.1}$$

Experiment	t (s)	UH (m²/s) from experiment	UH (m²/s) from (2.2)
1	100	0.016	0.022
2	130	0.018	0.017
3	90	0.0093	0.0092
4	210	0.016	0.015
5	160	0.022	0.021
6	200	0.012	0.014

TABLE 2. Observed and calculated flow rates

where the 'model constant' $c \approx 5$ (different values are mentioned in the literature). The more-or-less linear growth of H/H_0 observed when $t > t_1$ (experiments 1–5) indicates that the entrainment process then has become fully developed.

The density profiles taken during these experiments suffered from instrumental imperfections, so that reliable quantitative results could not be obtained. However, the relatively deep transition layers observed in the experiments with recirculation (§3.2) also occurred in experiments 1–5.

In table 2 observed flow rates per unit width (UH) in the upper layer are compared with the flow rates given by the equation of motion (2.2). The friction velocities under homogeneous conditions (table 1) were assumed to remain unaltered. Owing to the external waves mentioned above, the observed velocity U has to be taken relative to the (almost uniform) velocity of the return flow in the lower layer. It is seen in table 2 that in experiments 2–6 the agreement is good. In experiment 1 the high air velocity caused substantial internal-wave disturbances. The lower observed UH in this experiment can be, at least partly, attributed to drag exerted by these waves. Despite the lower flow rate in experiment 1, there seems to be no reason to assume that stratification affects the friction velocity.

3.2. *Experiments with recirculation*

The experiments with recirculation were done to suppress the influence of the endwalls, thus increasing the maximal duration of an experiment. Experiments at larger values of Ri_* then become feasible. The experiments carried out are listed in table 3.† The required and observed rates of recirculating flow are shown in figure 4.

Molecular effects are likely to be unimportant in these experiments (as in the experiments of §3.1). Reynolds numbers UH/ν varied from about 0.9×10^4 to 4×10^4 during the periods of active mixing, and the Péclet numbers are much larger because of the small diffusivity of salt in water. The duration of the experiments was relatively short (less than twenty minutes), but long enough for the entrainment process to become fully developed: the timescale t_1 given by (3.1) varies from about 60 s (experiment 7) to 560 s (experiment 12).

3.2.1. *Visual observations*

The shadowgraph images filmed near the middle of the flume showed that in the experiments with large Ri_* (nos. 10–12) the recirculation procedure worked properly. The experiments reproduced well, internal waves of some significance were not

† The friction velocities in experiments 10–12 have been reduced by the factor discussed at the end of §2.4. This factor was evaluated for the phase of the experiments in which the entrainment process had become fully developed (the upper-layer velocity U is then more-or-less constant).

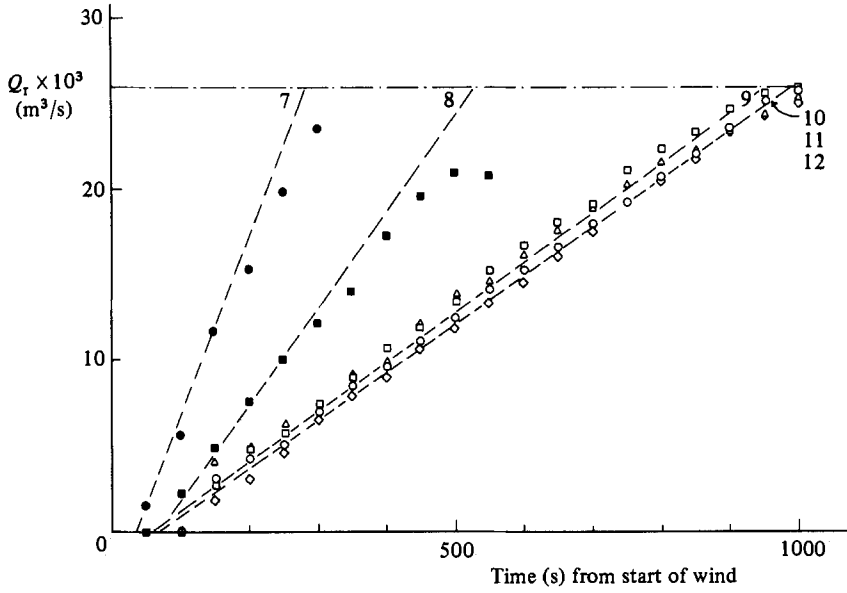

FIGURE 4. Rate of recirculating flow: ●, experiment 7; ■, 8; ○, 9; □, 10; △, 11; ◇, 12; ---, required flow rate according to (2.2), experiment numbers are shown; -·-·-, maximal flow rate. The low value in experiment 8 at 550 s is caused by the arrival of the wave disturbance (§3.2) at the skimmer valve.

Experiment	$u_{0.1}$ (m/s)	u_* (mm/s)	H_0 (m)	$\frac{\Delta\rho_0}{\rho_r}$	Ri_*
7	8.6	11.4	0.10	0.0053	40
8	6.4	8.4	0.10	0.0048	67
9	4.3	6.0	0.10	0.0049	130
10	4.3	5.9	0.10	0.0096	270
11	4.3	5.9	0.10	0.019	540
12	4.3	5.9	0.10	0.039	1090

TABLE 3. Experiments with recirculation

observed, and the oil drops rising in the lower layer indicated that little or no motion occurred in this layer. In experiments 8 and 9 a single large-amplitude internal wave, disturbing the interface and vertical velocity distribution, travelled in the downstream direction through the measuring section about 250–400 s after the recirculation had been started. Such a wave was also observed in experiment 7 (at $t \approx 250$ s), but in this case the maximal rate of recirculating flow (§2.1) had already been reached before the wave appeared. This wave phenomenon seems to be inherent to the experimental set-up: when experiments 7–9 were repeated, a similar wave was observed at about the same time. It seems to be generated by a transition from internally subcritical flow to supercritical flow at the upstream end of the flume. About 170 s (the travelling time) after the flow became supercritical in experiments 7–9, the wave arrived at the measuring section. The flow remained subcritical or nearly critical in experiments 10–12.

The filmed shadowgraph images give rise to the following comments on the structure of the upper layer in the experiments done.

Experiment 7. Initially, little difference was observed between mixed layer and transition layer, both layers being turbulent. In the transition layer rotating structures intermittently produced inverted turbulent 'boils' at the interface which protruded into the lower layer. These boils remained connected to the upper layer, retreated, and then disappeared completely. In a later phase the transition layer was less turbulent, and its relative thickness seemed to decrease somewhat.

Experiment 8. A mixed layer and a transition layer could be discerned throughout the experiment. In the latter layer elongated rotating structures developed, which initially had an inclination to the horizontal, but later turned to the horizontal direction. Boils were less frequent, and highly unsteady 'filaments' of upper-layer water just below the interface were observed. In course of time the relative thickness of the transition layer and the turbulence intensity in this layer decreased.

Experiment 9. The behaviour was more or less as in experiment 8, but the intensity of the turbulence was less.

Experiment 10. The interface between the transition layer and the lower layer was more pronounced than in the previous experiments, in particular in the initial phase of the experiment. The elongated structures in the transition layer were nearly horizontal throughout the experiment. Occasionally wave breaking occurred at the interface. Filaments were observed, but boils were not. In later stages a stable transition layer developed. The vertical scale of the density structures in the transition layer was significantly less than the thickness of this layer.

Experiment 11. The behaviour was about the same as in experiment 10, but the turbulence intensity had decreased further. A stable interface existed during a long (initial) phase of the experiment. Relatively large turbulent structures on the boundary between mixed layer and transition layer were visible.

Experiment 12. Initially the interface was stable, and mixing started at a distinct instant ($t \approx 600$ s). The transition layer that then developed remained relatively shallow and showed only horizontal structures. Occasionally filaments and small turbulent 'clouds' just below the interface were observed. Sometimes the interface was wavy. No interaction between mixed layer and transition layer was visible.

In experiments 9–12 periods with little mixing were interspersed with periods of more vigorous mixing. Because of the initially diffused interface, Kelvin–Helmholtz billows were not observed during the early phases of the experiments.

3.2.2. *Results of measurements*

The depths H of the upper layer were read from the filmed shadowgraph images. The results in figures 5(*a–f*) are not presented in dimensionless form (as in figure 3), since at larger Ri_* the influence of recirculation would prevent a collapse of dimensionless data. The instants at which the linear relationship between rate of recirculating flow and time ((2.2) and figure 4) is no longer valid are indicated. The data shown beyond these instants are thought to be not yet affected by wave reflections from the end walls.

The initial depth of the upper layer was 0.10 m in all experiments, but because of molecular diffusion the initial thickness of the interlayer was about 0.06 m. Turbulence rapidly penetrated into this layer, which explains the relatively large upper-layer depths at small times shown in figures 5(*a–e*).

As expected, the time for the entrainment process to become fully developed increases, and the entrainment rate decreases, as Ri_* increases. The decrease in entrainment rate w_e is, however, only moderate ($w_e/u_* \approx 0.08$ when $Ri_* = 40$, and $w_e/u_* \approx 0.036$ when $Ri_* = 1090$). It is shown in §3.3 that entrance mixing owing to

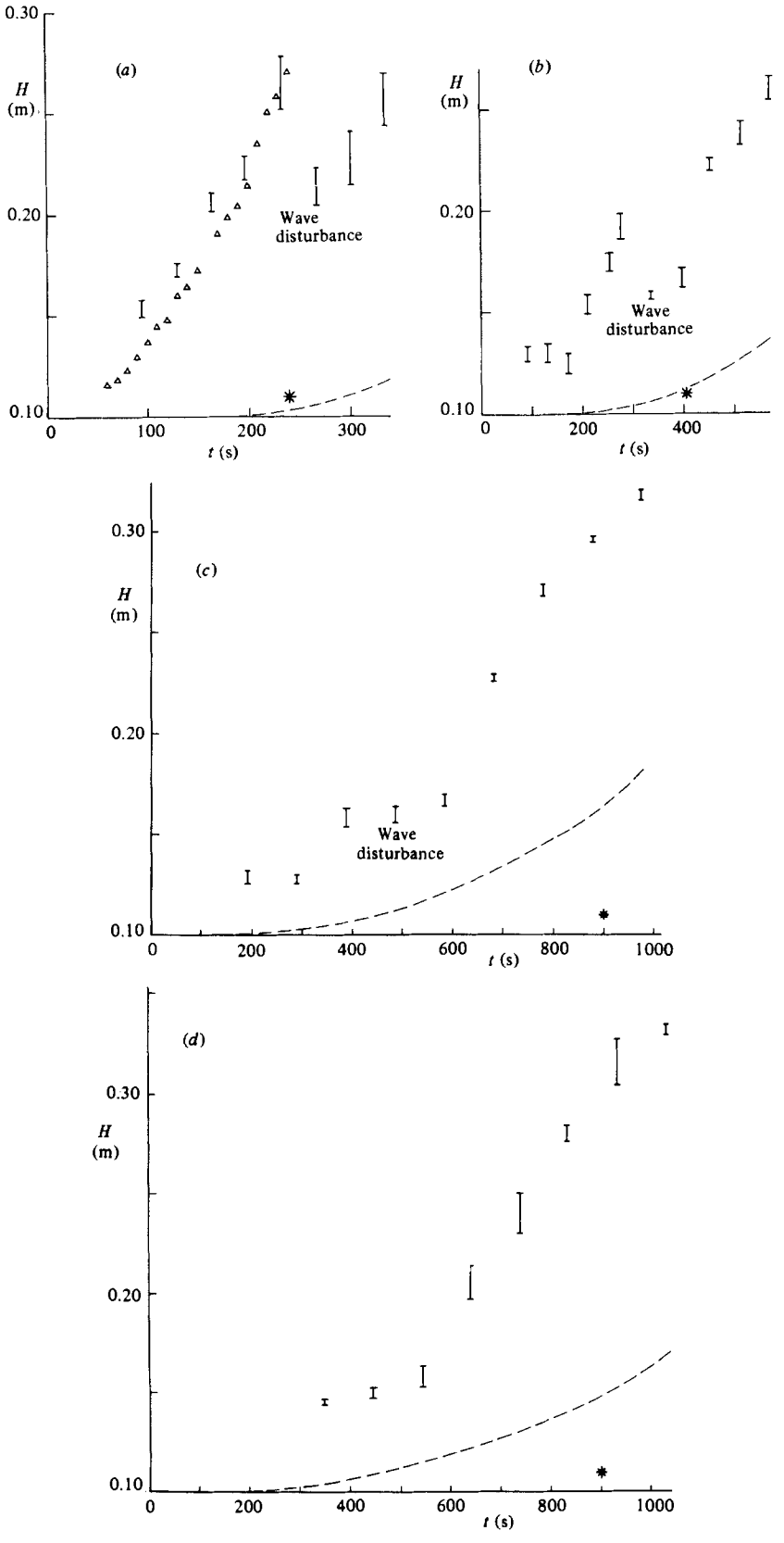
(a)
H (m)
0.30
0.20
0.10
Wave disturbance
0
100
200
300
t (s)
(b)
H (m)
0.20
0.10
Wave disturbance
0
200
400
t (s)
(c)
H (m)
0.30
0.20
0.10
Wave disturbance
0
200
400
600
800
1000
t (s)
(d)
H (m)
0.30
0.20
0.10
0
200
400
600
800
1000
t (s)

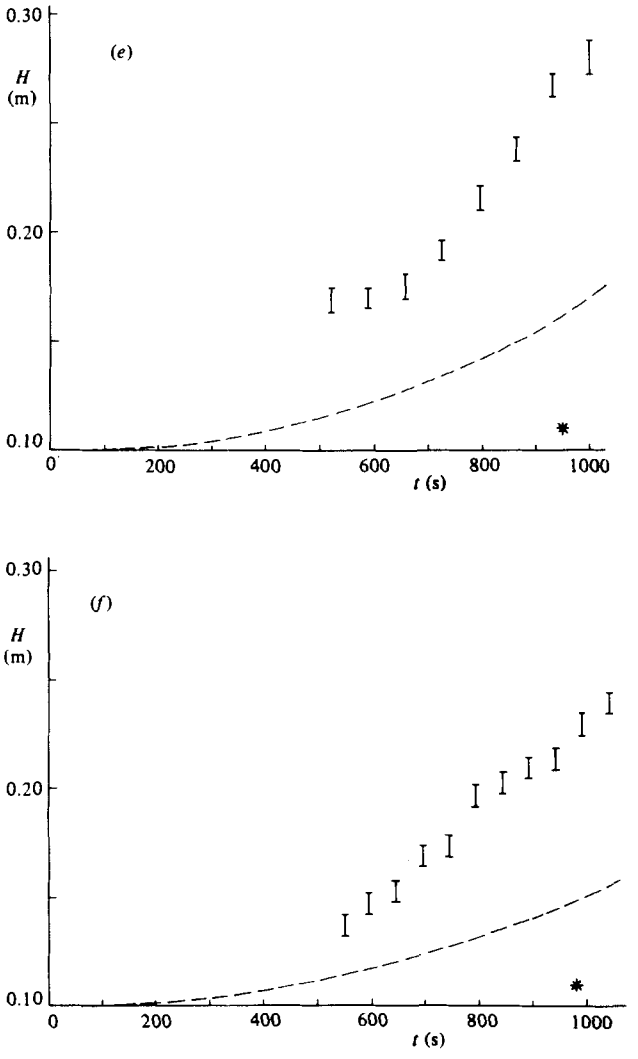

FIGURE 5. Upper-layer depths in experiments with recirculation: (*a*) experiments 7 and 2 (triangles); (*b*) 8; (*c*) 9; (*d*) 10; (*e*) 11; (*f*) 12; *, instant at which (2.2) is no longer satisfied; ——, calculated contribution H_r of entrance mixing to upper-layer depth (§3.3).

the recirculation applied causes the relatively large entrainment rates at large Ri_*. The possible influence of sidewall drag is discussed in §4.

The upper-layer depths of experiment 2 and 7 (both having $Ri_* = 40$) shown in figure 5 (*a*) are nearly the same, despite the recirculation applied in experiment 7. The explanation is, that at low values of Ri_* the influence of recirculation is small, partly since wind mixing then is dominant, and partly since the influence of entrance mixing reaches the measuring section only after a certain travelling time (see also §3.3).

As an example, figure 6 shows mean-density and mean-velocity profiles of experiment 10. These profiles are representative of all experiments. The measured profiles are not unlike those calculated by Mellor & Strub (1980) and Kundu (1981)

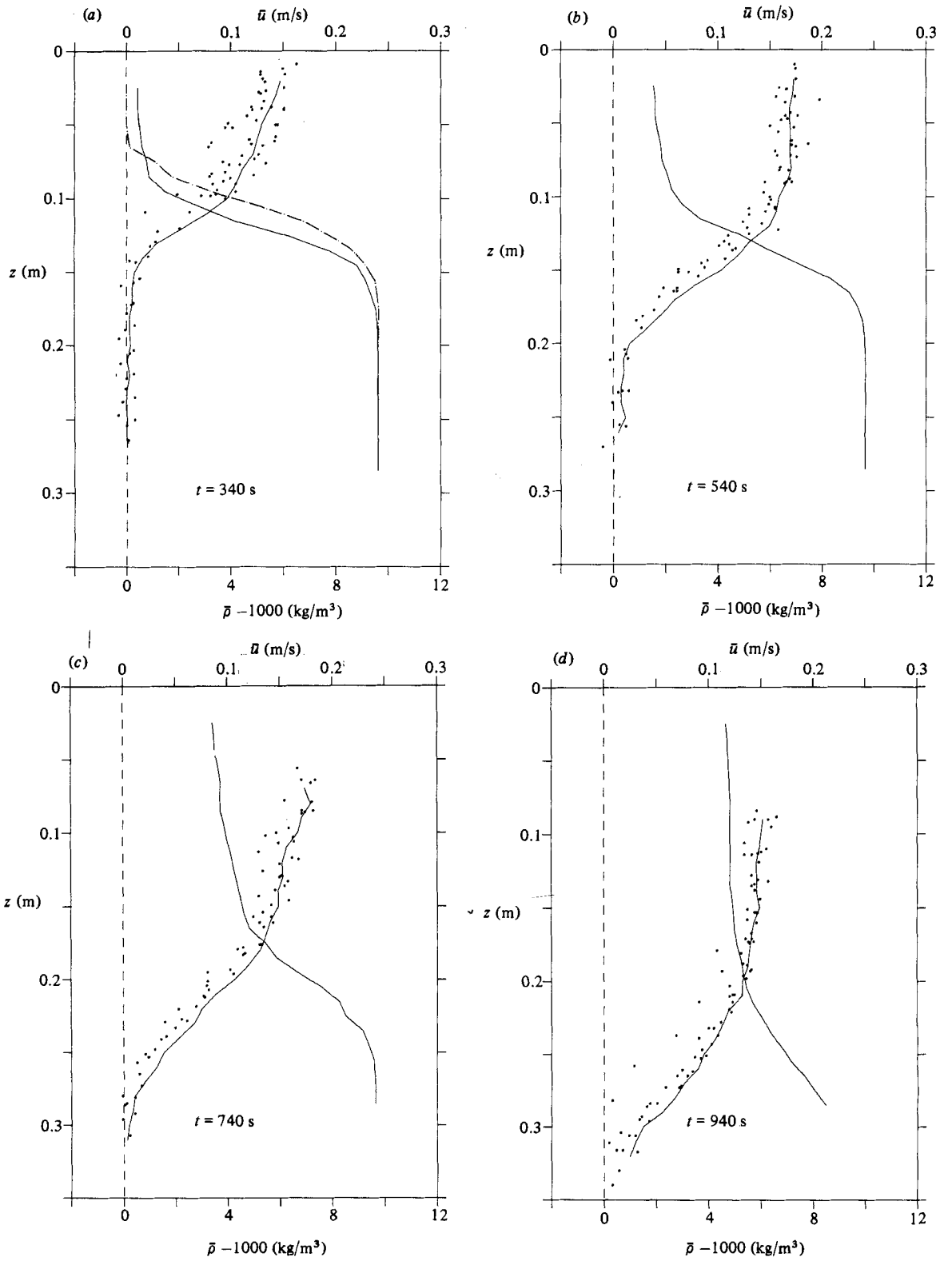

FIGURE 6. Mean-density and mean-velocity profiles of experiment 10: dots represent velocities of individual oil drops; –·–·–·–, initial density profile. See figure 1 for notation.

	Profile			
Experiment	1	2	3	4
7	130	200	270	340
8	270	390	510	630
9	280	480	680	880
10	340	540	740	940
11	580	720	860	1000
12	640	740	840	940

TABLE 4. Instants at which profiles were aken (time in s)

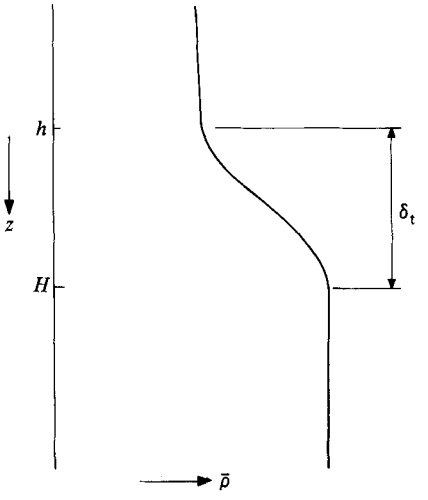

FIGURE 7. Definition sketch of thickness δ_t of transition layer.

using higher-order turbulence models. In particular, the calculations also show the relatively deep transition layers observed in the present experiments.

The instants at which the profiles were taken are listed in table 4. The upper 2.5 cm of the density profiles are not shown, since the conductivity probe used produces a systematic error when used near a free surface (or a solid wall). The profiles of experiments 7 and 8 showed an influence of the wave disturbance mentioned.

Apart from one or two profiles of experiment 7, the density profiles showed a mixed layer with relatively little density differences and a transition layer with larger density gradients. Thicknesses δ_t (as defined in figure 7) of the transition layer and density gradients $\partial\bar{\rho}/\partial z$ were estimated from the density profiles taken during upward and downward traverses of the probe and then averaged (estimating δ_t from the averaged density profiles as shown in figure 6 sometimes required more judgement). Ratios of thickness δ_t to upper-layer depth are given in table 5. The ratio δ_t/H seems to decrease with increasing Ri_* and, in most cases, during an experiment. However, the values are considerably larger than those in the two-layer experiments of Deardorff & Willis (1982).

The velocities of individual oil drops were averaged locally to give smooth profiles. Profiles corrected for inertia of the oil drops are shown in figure 6. In several cases only partial profiles were obtained, since the oil drops then had travelled too far

	Profile				
Experiment	1	2	3	4	Mean
7	0.69	1	0.73	0.57	0.77
8	0.73	0.71	0.52	0.52	0.62
9	0.69	0.74	0.58	0.47	0.62
10	0.63	0.53	0.42	0.42	0.50
11	0.52	0.56	0.47	0.48	0.51
12	0.38	0.35	0.37	0.47	0.39

TABLE 5. Relative thickness δ_t/H of interlayer

		Ri_t, Profile					
Experiment	k_s	1	2	3	4	Mean	Ri_m
7	0.31	0.28	0.19	0.29	0.16†	0.23	0.05–0.2
8	0.39	0.37	0.28	0.25	0.29	0.30	0–0.3
9	0.33	0.26	0.23	0.28	0.25	0.26	0.06–0.4
10	0.34	0.80‡	0.66‡	0.43	0.38	0.41	0.07–0.8
11	0.35	0.75‡	0.46	0.47	0.49	0.47	0.2–> 1
12	0.42	1.0‡	0.64	0.72	0.68	0.68	0.5–> 1

† Not accurate.

‡ Presumably the high value is caused by the fact that the entrainment process was not yet fully developed. This value was disregarded at averaging.

Table 6. Coefficients k_s and gradient Richardson numbers Ri_t and Ri_m

downstream. The surface drift velocities u_s were larger than those observed under homogeneous conditions because of the recirculating flow in the upper layer. The coefficients k_s defined by $u_s = U + k_s u_{*a}$ are listed in table 6. Under homogeneous conditions u_s was about $0.55u_{*a}$.

A weak flow against the wind was observed in the lower layer in experiments 11 and 12. Presumably this flow is caused by entrance mixing near the inlet box (see §3.3).

In general there is a close relation between density and velocity profiles. In particular, the thicknesses of the interlayer are approximately the same in most cases. An exception was profile 3 of experiment 12, where the velocity profile showed a thicker interlayer than the density profile. The waviness of the interface mentioned before may have been responsible for this.

Gradient Richardson numbers Ri defined by

$$Ri = \frac{g\,\partial\bar{\rho}/\partial z}{\rho_r(\partial\bar{u}/\partial z)^2} \tag{3.2}$$

were determined from these profiles. Richardson numbers Ri_t in the transition layer where the gradients are maximal are shown in table 6. Remarkably, Ri_t increases with Ri_*. The mean values found in experiments 7–9 are in the same range as those obtained by Wyatt (1978) and Koop & Browand (1979). The larger values in experiments 10–12 are related to the recirculation (see §3.3).

Gradient Richardson numbers Ri_m in the mixed layer below the surface shear layer

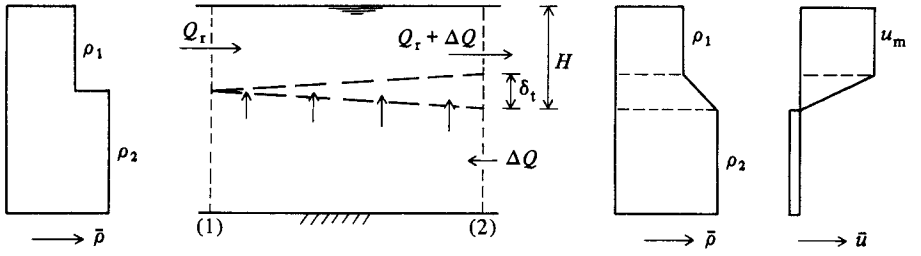

FIGURE 8. Schematic diagram of entrance mixing. The recirculating flow enters the flume in cross-section (1); the density and velocity profiles are fully developed in cross-section (2).

were also estimated. Results of some accuracy are difficult to obtain because of the small gradients in this layer. Surprisingly the values found (table 6) were not always small when compared with those in the transition layer. This seems to be particularly true in the experiments with large Ri_*. This result would indicate that the turbulence in the mixed layer is also affected by buoyancy, at least intermittently.

3.3. *Corrections for entrance mixing in experiments with recirculation*

The water withdrawn downstream is completely mixed in the recirculation system before it is discharged upstream. The inflowing upper-layer water is therefore homogeneous, and near the entrance the flow will be subject to Kelvin–Helmholtz-type instability (besides wind-induced mixing) to form a transition layer of thickness δ_t. As a consequence of this entrance mixing, water from the lower layer is locally entrained into the upper layer. The withdrawal of water from the lower layer speeds up the growth of the upper layer in the whole flume. The aim of this section therefore is to correct the entrainment rates w_e and gradient Richardson numbers Ri_t of the transition layer for the effects of entrance mixing.

Figure 8 shows a schematic diagram of the region where the entrance mixing takes place and the transition layer is formed. The inflow comes into contact with the lower layer in cross-section (1), and the entrance mixing is completed in cross-section (2). Assuming the density and velocity profiles shown, the continuity equation† and mass balance give, when applied to the region between cross-sections (1) and (2),

$$Q_r + \Delta Q = (H - \tfrac{1}{2}\delta_t)\, W u_m, \tag{3.3}$$

$$\rho_1 Q_r + \rho_2 \Delta Q = [\rho_1 (H - \tfrac{1}{2}\delta_t) + \tfrac{1}{6}(\rho_2 - \rho_1)\, \delta_t]\, W u_m, \tag{3.4}$$

where ΔQ is the volume flux of water entrained from the lower layer, u_m the velocity of the mixed layer, and ρ_1 and ρ_2 are the densities of the mixed and undisturbed layers. Eliminating u_m between (3.3) and (3.4) gives

$$\frac{\Delta Q}{Q_r} = \frac{\delta_t / H}{6 - 4\delta_t / H}. \tag{3.5}$$

The part H_r of the upper-layer depth that is related to entrance mixing is given by

$$\frac{\mathrm{d}H_r}{\mathrm{d}t} = \frac{\Delta Q}{Wl}, \tag{3.6}$$

† It is easily shown that replacing the salinity balance by the continuity equation is a good approximation in this case.

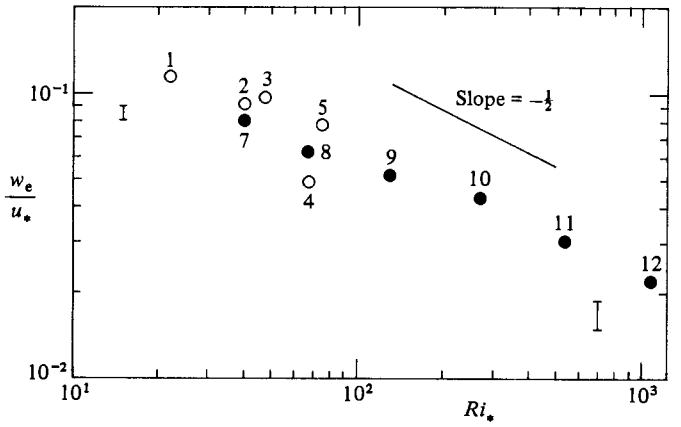

FIGURE 9. Dimensionless entrainment rates w_e/u_* versus Ri_*: ○, experiments without recirculation; ●, experiments with recirculation, corrected for entrance mixing. Experiment numbers are shown.

where L is the effective length of the flume. Substituting from (2.2) and (3.5), (3.6) gives (assuming $Q = Q_r$ and δ_t/H = constant)

$$H_r = \frac{1}{2}\frac{\delta_t/H}{6-4\delta_t/H}\frac{u_*^2 t^2}{L}. \tag{3.7}$$

The depths H_r were calculated for experiments 7–12 using table 5, and the results are plotted on figures 5(*a–f*) (dashed curves). Since the influence of entrance mixing becomes noticeable at the measuring section only after a certain travelling time, the time axes were shifted accordingly (time delays of 170 s for experiments 7–9, 120 s for experiment 10, 80 s for experiment 11, and 60 s for experiment 12).

Entrance mixing is negligible in experiment 7 (the results of experiments 7 and 2 therefore agree – see figure 5*a*) and becomes increasingly important in experiments 8–12. In experiment 12 the contribution of entrance mixing to the total deepening of the upper layer amounts to about 40 %.

Entrainment rates w_e during the fully developed phase of the mixing process were corrected for entrance mixing using figure 5 and the relation $w_e = \mathrm{d}(H-H_r)/\mathrm{d}t$. The results are shown in figure 9, together with the entrainment rates obtained from experiments 1–5. Although the data show considerable scatter, the entrainment rates are reasonably well represented by the expression

$$\frac{w_e}{u_*} \approx (0.6 \pm 0.1)\, Ri_*^{-\frac{1}{2}}. \tag{3.8}$$

The results obtained are similar to those of Price (1979*a*) and Thompson (1979). These authors extrapolated the experimental results of Kantha *et al.* (1977) to zero aspect ratio and found $w_e/u_* \approx 0.7 Ri_*^{-\frac{1}{2}}$ to $0.9 Ri_*^{-\frac{1}{2}}$. The turbulence model employed by Mellor & Strub (1980) produced a result nearly identical with (3.8) (no entrainment rates for $Ri_* > 400$ are shown, however). Similar results were obtained by Kundu (1981) and Kranenburg (1983). The integral entrainment model of Spigel & Imberger (1980) also predicts the $Ri_*^{-\frac{1}{2}}$ behaviour.

The gradient Richardson number Ri_t of the transition layer can be written (see the definition (3.2))

$$Ri_t \approx \frac{g}{\rho_r}\frac{\Delta\rho_0 H_0/H\delta_t}{(u_m/\delta_t)^2} \approx \frac{\Delta\rho_0 g H_0}{\rho_r U^2}\frac{\delta_t}{H}\left(1-\frac{1}{2}\frac{\delta_t}{H}\right)^2.$$

Experiment	7	8	9	10	11	12	Mean
$\left(\frac{H-H_r}{H}\right)^2 Ri_t$	0.23	0.23	0.18	0.24	0.18	0.28	0.22

TABLE 7. Gradient Richardson number of transition layer corrected for entrance mixing

Substituting from (2.2) gives

$$Ri_t \approx Ri_* \left(\frac{H}{u_* t}\right)^2 \frac{\delta_t}{H}\left(1-\frac{1}{2}\frac{\delta_t}{H}\right)^2. \tag{3.9}$$

The experimental ratio δ_t/H is likely to be determined mainly by the wind-induced mixing, since it increases neither significantly with time nor with Ri_* (see table 5), as opposed to the influence of entrance mixing. Also, the similarity profiles for density and velocity proposed in the literature imply a time-independent value of δ_t/H. Since, furthermore, Ri_t is only weakly dependent on δ_t/H for the values given in table 5, (3.9) shows that at a particular instant Ri_t is approximately proportional to H^2. Consequently, the experimental values of Ri_t (table 6) can be corrected for the influence of entrance mixing by multiplying by $(H-H_r)^2/H^2$. This operation, the results of which are shown in table 7, removes the tendency of Ri_t to increase with Ri_*. The mean value (0.22) is less than that obtained by Piat & Hopfinger (1981) in a somewhat different set-up. These authors found $Ri_t \approx 0.33$, but did not consider possible entrance effects. Price (1979*b*) estimated $Ri_t \approx 0.26$ for a rain-formed mixed layer.

4. Summary and discussion

The experimental set-up employed aimed at simulating wind mixing in a situation where the endwalls do not yet affect the mixing using a rectilinear configuration. As a consequence curvature effects as encountered in annular tanks were absent. To eliminate the influence of the endwalls, water from the upper layer had to be recirculated at larger values of Ri_*. The additional mixing caused by recirculation was found to be non-negligible. The extrapolation to the situation where recirculation is absent was found to be rather straightforward, whereas the extrapolation to zero curvature of results obtained in an annular tank is difficult, if indeed it is possible at all.

The observed mean density and velocity profiles as well as visual observations showed the development of a mixed layer with little density differences and a transition layer with relatively large density and velocity gradients. In all experiments the transition layer occupied a considerable part of the total upper layer. The surface shear layer was less developed than in the case of homogeneous flow. As judged from the gradient Richardson number, the turbulence in the transition layer is in a near-critical condition when recirculation is absent. Estimates of the gradient Richardson number in the mixed layer indicate that buoyancy influences the dynamics in this layer also, at least at larger Ri_*. Shadowgraph images showed large-scale structures in the transition layer, whereas the mixed layer appeared more uniform. The entrainment process seems to be dominated by mixing in 'boils', highly turbulent patches temporarily protruding into the undisturbed layer, when Ri_* is small. Intermittent small-scale wave breaking, producing 'filaments' and small 'clouds', was observed when Ri_* was large.

In view of the experience gained with annular tanks, the question arises as to what extent sidewall drag has influenced the experimental results. In the experiments without recirculation wall friction would tend to reduce the entrainment rates, as in experiments in annular tanks. However, in the experiments with recirculation, the flow rates satisfied (2.2), which is also satisfied in a situation without wall friction. As a result, wall drag may have enhanced the mixing in the upper layer (although the shadowgraph images did not reveal such behaviour). If this is true, wall drag could have *increased* the entrainment rates in these experiments. Figure 9 shows, however, that the entrainment rates in experiments 1–5 are not significantly less than those in experiments 7–9, indicating that wall drag was not important in experiments 1–9. Attempts are not made here to correct the entrainment rates of experiments 10–12 for possible (presumably small) effects of wall drag.

The author wishes to thank the members of the Laboratory of Fluid Mechanics, Department of Civil Engineering, Delft University of Technology, for their assistance. In particular he is indebted to Mr A. M. den Toom, who conducted the experiments.

REFERENCES

DEARDORFF, J. W. & WILLIS, G. E. 1982 Dependence of mixed-layer entrainment on shear stress and velocity jump. *J. Fluid Mech.* **115**, 123–150.

IMBERGER, J. & HAMBLIN, P. F. 1982 Dynamics of lakes, reservoirs, and cooling ponds. *Ann. Rev. Fluid Mech.* **14**, 153–187.

JONES, I. S. F. & MULHEARN, P. J. 1983 The influence of external turbulence on sheared interfaces. *Geophys. Astrophys. Fluid Dyn.* **24**, 49–62.

KANTHA, L. H., PHILLIPS, O. M. & AZAD, R. S. 1977 On turbulent entrainment at a stable density interface. *J. Fluid Mech.* **79**, 753–768.

KATO, H. & PHILLIPS, O. M. 1969 On the penetration of a turbulent layer into stratified fluid. *J. Fluid Mech.* **37**, 643–655.

KOOP, C. G. & BROWAND, F. K. 1979 Instability and turbulence in a stratified fluid with shear. *J. Fluid Mech.* **93**, 135–159.

KRANENBURG, C. 1983 The influence of side-wall friction on shear-stress driven entrainment experiments. *J. Hydraul. Res.* **21**, 99–117.

KUNDU, P. K. 1980 A numerical investigation of mixed-layer dynamics. *J. Phys. Oceanogr.* **10**, 220–236.

KUNDU, P. K. 1981 Self-similarity in stress-driven entrainment experiments. *J. Geophys. Res.* **86**, 1979–1988.

MELLOR, G. L. & STRUB, P. T. 1980 Similarity solutions for the stratified turbulent Rayleigh problem. *J. Phys. Oceanogr.* **10**, 455–460.

MITSUYASU, H. & HONDA, T. 1982 Wind-induced growth of water waves. *J. Fluid Mech.* **123**, 425–442.

MOORE, M. J. & LONG, R. R. 1971 An experimental investigation of turbulent stratified shearing flow. *J. Fluid Mech.* **49**, 635–655.

PHILLIPS, O. M. & BANNER, M. L. 1974 Wave breaking in the presence of wind drift and swell. *J. Fluid Mech.* **66**, 625–640.

PIAT, J.-F. & HOPFINGER, E. J. 1981 A boundary layer topped by a density interface. *J. Fluid Mech.* **113**, 411–432.

PRICE, J. F. 1979*a* On the scaling of stress-driven entrainment experiments. *J. Fluid Mech.* **90**, 509–529.

PRICE, J. F. 1979*b* Observations of a rain-formed mixed layer. *J. Phys. Oceanogr.* **9**, 643–649.

SCRANTON, D. R. & LINDBERG, W. R. 1983 An experimental study of entraining, stress driven, stratified flow in an annulus. *Phys. Fluids* **26**, 1198–1205.

SPIGEL, R. H. & IMBERGER, J. 1980 The classification of mixed-layer dynamics in lakes of small to medium size. *J. Phys. Oceanogr.* **10**, 1104–1121.

THOMPSON, R. O. R. Y. 1979 A reinterpretation of the entrainment process in some laboratory experiments. *Dyn. Atmos. Oceans* **4**, 45–55.

THORPE, S. A. 1968 A method of producing a shear flow in a stratified fluid. *J. Fluid Mech.* **32**, 693–704.

WU, J. 1973 Wind-induced turbulent entrainment across a stable density interface. *J. Fluid Mech.* **61**, 275–287.

WU, J. 1975 Wind-induced drift currents. *J. Fluid Mech.* **68**, 49–70.

WYATT, L. R. 1978 The entrainment interface in a stratified fluid. *J. Fluid Mech.* **86**, 293–312.